Numerical Methods in Civil Engineering, 10-1 (2025) 82-101

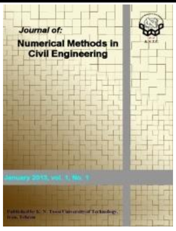

Numerical Methods in Civil Engineering

Journal Homepage: https://nmce.kntu.ac.ir/

Seismic Retrofitting of Corner RC Beam-Column Joints with Floor Slab: Numerical Assessment of Hybrid and Composite Systems

Rusul Sfoog Humairy*, Mahdi Sharifi **, Rouhollah Amirabadi *, Mohamad Reza Shokrzadeh**

ARTICLE INFO

RESEARCH PAPER

Article history:
Received:
August 2025
Revised:
September 2025
Accepted:
October 2025

Keywords:
Seismic retrofitting, corner RC beam-column joint, floor slab effect, hybrid strengthening systems, plastic strain index

Abstract:

This paper presents a finite element investigation into the seismic performance and retrofitting of corner RC beam-column joints with an attached floor slab—a realistic detail often neglected in previous studies. Seven models, including code-compliant, non-ductile, and five advanced retrofitting configurations (external steel cages, bolted steel boxes, externally bonded CFRP, and hybrid steel–FRP systems), were analyzed under monotonic loading using a calibrated damage plasticity approach. Explicit modeling of the slab–joint interaction enabled a realistic assessment of strength, ductility, and damage control. Results indicate that hybrid retrofitting strategies, particularly CFRP-BSB and BSAC, significantly enhance both ductility and damage mitigation, matching or surpassing the performance of code-compliant specimens. CFRP-only and CFRP-NSM systems also provided substantial gains in energy dissipation and control of inelastic damage, while the BSB method, despite increased strength, showed greater localization of plastic strains. Analysis of the principal plastic strain index and force–displacement curves highlights the value of integrated composite and steel confinement in restoring seismic resilience to vulnerable joints. These findings provide practical recommendations for the seismic upgrade of existing RC beam-column joint with floor slabs, emphasizing the importance of considering slab effects, advanced hybrid retrofitting, and robust damage indices in retrofit design and assessment.

1. Introduction

Over the past decades, seismic events worldwide have exposed the vulnerability of reinforced concrete (RC) structures, particularly those with non-ductile frames designed and constructed before the enforcement of modern seismic codes [1–3]. Catastrophic failures in Turkey, Indonesia, Iran, and other seismic regions have consistently demonstrated that buildings lacking adequate seismic detailing, especially at critical connections such as beam-column joints, are highly susceptible to brittle failures during earthquakes [3,4]. In Iraq, the prevalence of RC buildings constructed according to outdated design practices further raises concerns regarding their capacity to withstand seismic demands [5]. These structures often lack essential features such as sufficient confinement reinforcement, proper anchorage of longitudinal bars, and adequate transverse reinforcement in joint cores. As a result, their energy dissipation capacity and ductility are significantly compromised [1]. The seismic performance of RC frames is largely governed by the integrity of their beam-column joints [2,3]. When subjected to strong ground motions, deficiencies in joint detailing—such as inadequate lap splices, insufficient transverse reinforcement, and improper anchorage—can lead to joint shear failure, rebar slippage, and ultimately, loss of structural integrity [4,5]. Observations from post-earthquake investigations have underscored that many failures originate within these joints, even when beams and columns remain relatively undamaged [6–9]. Moreover, the lack of proper joint confinement and energy dissipation mechanisms further exacerbates the risk of collapse, posing significant threats to human life and economic stability [3,10–12]. Retrofitting and strengthening deficient RC beam-column joints have, therefore, become a critical focus for enhancing

** Department of Civil Engineering, Faculty of Engineering, University of Qom, Qom, Tehran*
***Corresponding author: Department of Civil Engineering, Faculty of Engineering, University of Qom, Qom, Tehran*
**** International Institute of Earthquake Engineering and Seismology, Tehran, Iran*

https://doi.org/10.61882/NMCE.2508.1098

the seismic resilience of existing structures [10,13]. Conventional methods such as reinforced concrete jacketing and steel jacketing have proven effective in increasing joint strength and ductility, but they are often labor-intensive, increase the cross-sectional size and weight of the member, and can be difficult to implement in practice especially in structures with architectural constraints or limited access [14–21]. In response, researchers have increasingly turned to advanced materials and innovative retrofitting techniques, such as fiber-reinforced polymer (FRP) composites, near-surface mounted (NSM) reinforcements, and hybrid systems that integrate steel and FRP elements [18, 22–31]. These modern approaches offer several advantages, including higher strength-to-weight ratios, ease of installation, improved corrosion resistance, and minimal disruption to building use [2,18]. Despite the progress achieved in laboratory research, several important gaps remain. Most notably, there is a lack of comprehensive numerical studies that systematically assess the seismic behavior of retrofitted non-ductile RC beam-column joints under realistic conditions, including the influence of slabs, transverse beams, and the combined effects of different retrofit strategies. This shortfall is particularly critical in countries such as Iraq, where experimental resources are limited, but the demand for efficient and cost-effective retrofitting solutions is urgent. In contemporary earthquake engineering research, advanced numerical modeling is increasingly recognized as an essential precursor to experimental work [32]. Conducting detailed simulations prior to laboratory testing enables researchers to optimize specimen design, refine retrofitting strategies, and predict structural behavior under various scenarios—ultimately reducing experimental costs and focusing laboratory efforts on the most promising solutions. In this study, numerical analysis is strategically employed as the first step, providing critical insights that inform and guide future experimental investigations. This research aims to bridge the identified gaps by conducting a detailed finite element (FE) investigation into the seismic retrofitting of deficient RC beam-column joints. Advanced FE models are developed that explicitly incorporate slab effects, common detailing deficiencies, and a variety of retrofitting scenarios—including steel cage confinement, GFRP wrapping with mechanical anchorage, and NSM reinforcement. The numerical models are validated against published experimental data and subsequently employed for comparative assessment of retrofit effectiveness, constructability, and feasibility under seismic loading. This integrated numerical assessment, explicitly considering slab effects and realistic structural deficiencies, represents a significant novelty. Particularly in regions with limited experimental resources, this simulation-driven framework provides a practical basis for optimizing retrofitting strategies and guiding future experimental investigations. The findings are intended to provide actionable insights for engineers and policymakers, supporting the development of safer and more resilient built environments in seismic-prone regions with similar construction practices.

1.1 Research Significance

The need for seismic upgrading of non-ductile reinforced concrete (RC) structures remains a critical challenge worldwide, especially in regions with large inventories of buildings constructed before the implementation of modern seismic codes. Laboratory testing of retrofitting solutions is often limited by high costs, resource constraints, and the complexity of replicating realistic structural conditions. This study employs advanced numerical modeling as a practical and efficient alternative for evaluating and optimizing retrofitting strategies in deficient RC beam-column joints. By systematically simulating the effects of various retrofit techniques and realistic joint configurations, the research provides robust guidance for engineers and decision-makers seeking effective, constructible, and cost-efficient solutions for seismic strengthening. The findings help bridge the gap between analytical research and real-world practice, supporting the development of safer and more resilient urban environments in earthquake-prone regions globally. This is particularly significant for countries in the Middle East and other developing regions, where cost-effective numerical approaches provide critical support for enhancing seismic resilience amid limited access to comprehensive experimental testing.

2. Model Validation

The objective of the model validation phase was to ensure that the numerical simulations accurately reflect experimental behavior, thereby establishing confidence in subsequent parametric studies. Validation was performed using experimental data from two authoritative studies, each corresponding to a specific retrofitting or detailing scenario relevant to this research. These studies were selected due to their comprehensive experimental data, well-documented test conditions, and relevance to the retrofit methods explored in this research.

The primary validation was based on the experimental results reported by Khodaei et al. [8], which included three representative corner beam-column joint specimens: SJ0 (code-compliant), SJ3 (non-seismic/defective), and RSJ3 (retrofitted). SJ0 is a code-compliant specimen constructed with full seismic detailing, including adequate transverse reinforcement within the joint core, proper anchorage length for all longitudinal beam reinforcement, and closely spaced stirrups in both beams and columns in accordance with modern seismic codes. This configuration, featuring an attached floor slab, ensures ductile behavior and the formation of a flexural plastic hinge in the beam away from the column face (see Fig. 1.a for details of geometry and reinforcement layout). SJ3 is a non-seismic, defective specimen characterized by the absence of transverse reinforcement within the joint core, increased spacing of stirrups in both beams and columns, and insufficient anchorage length (without end hooks) for the bottom longitudinal bars of the beam. This arrangement typically leads to brittle joint shear failure and slippage of beam reinforcement under lateral loading (see Fig. 1.b for reinforcement details and test setup). RSJ3 represents the SJ3 specimen retrofitted with a steel enlargement system (welded steel angles, stiffeners, and post-tensioned bars), providing enhanced confinement and joint shear strength, and is expected to significantly improve ductility and delay brittle failure modes (see Fig. 1.c for retrofitting configuration and specimen dimensions).

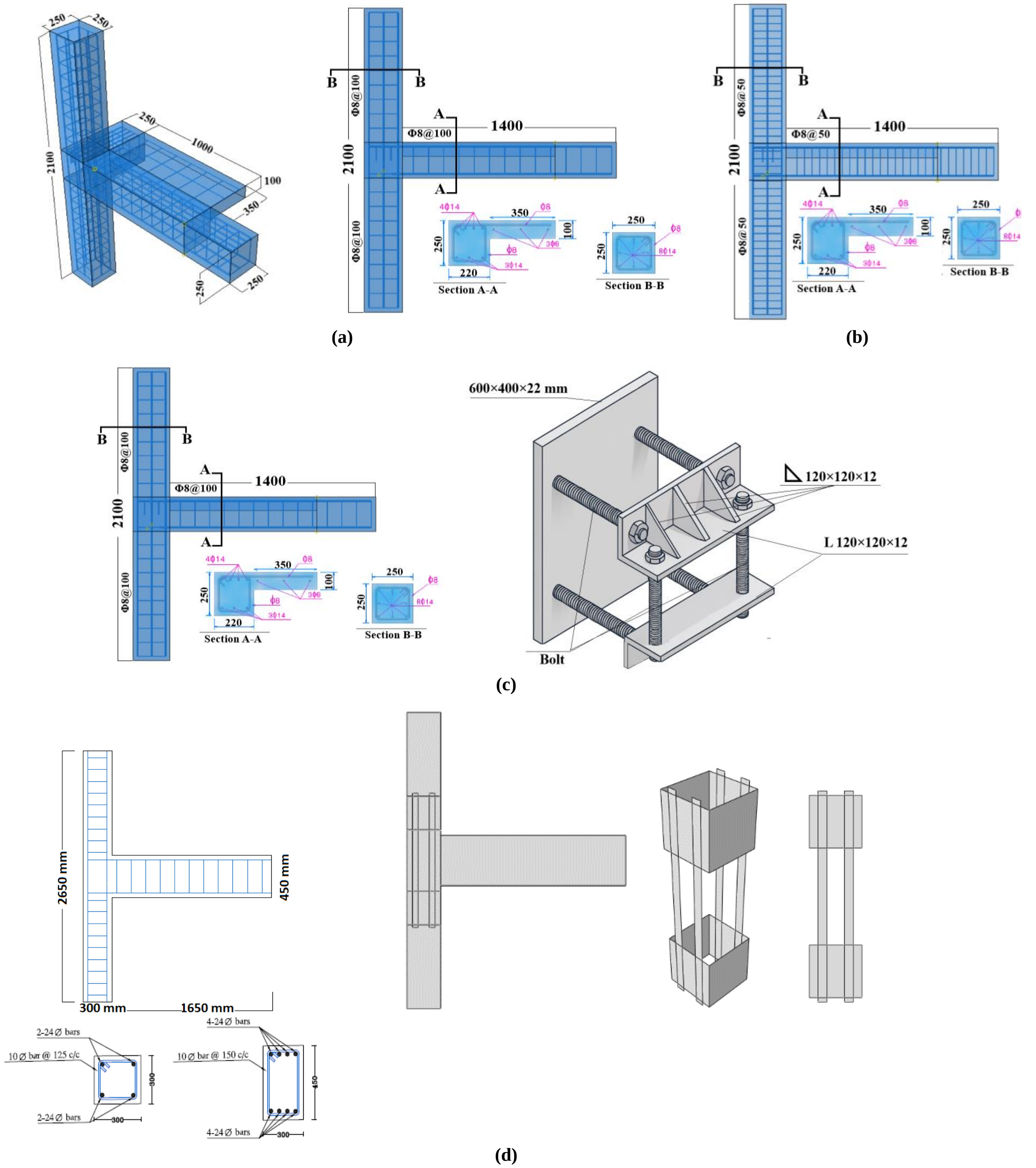

Fig.1: Schematic depiction of the beam and column sections utilized in the verification models [8,33]

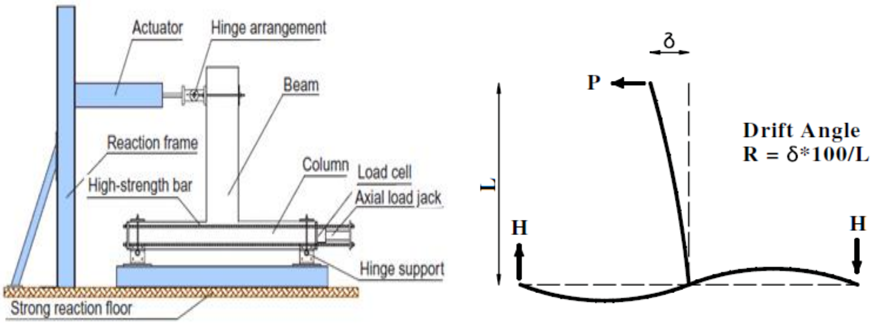

Fig. 2: Configuration of loading and support for the experimental specimen [8,33].

Additionally, to validate the ability of the numerical model to capture the behavior of joints retrofitted with fiber-reinforced polymers (FRP), the model was also compared to the experimental results of Shrestha et al. [33] (Fig. 1.d). In that reference study, an exterior RC beam-column joint—constructed without joint shear reinforcement—was strengthened with vertically oriented CFRP strips bonded to the joint region. The specimen, with a 28-day compressive strength of 25.4 MPa and appropriately detailed steel reinforcement, was tested under monotonic loading at the free end of the beam (Fig. 2). This case was particularly relevant as CFRP retrofitting was also used in the present study. All Khodaei specimens were subjected to quasi-static cyclic lateral loading applied at the free end of the beam, with a constant axial load on the column (Fig. 2).

For the purpose of model validation, the envelope of the experimental hysteresis curves (i.e., the monotonic backbone) was extracted and used to compare with the monotonic load–displacement responses obtained from the numerical simulations. The use of the monotonic envelope from experimental hysteresis curves ensures a consistent basis for comparison, simplifying the validation process while accurately capturing the critical response parameters under cyclic loading. The validation criterion adopted in this study required numerical results to show less than 5% deviation in peak loads and accurately capture failure modes observed in experimental studies.

3. Numerical models' description

Finite element analyses were conducted using ABAQUS [30] to simulate the behavior of RC beam-column joints tested in the referenced experiments. The Concrete Damage Plasticity (CDP) model was employed to accurately represent the nonlinear response of concrete, capturing both compressive crushing and tensile cracking failure mechanisms [18]. The model combines isotropic elasticity degradation with compressive plasticity and tensile cracking. Key CDP parameters were carefully selected based on detailed calibration studies and recommendations from the literature [18]. The adopted Concrete Damage Plasticity (CDP) parameters were carefully selected based on published recommendations and calibration against experimental data. A dilation angle of 30° was chosen following Kent and Park [34] and the ABAQUS User's Manual [35], as it provided a realistic balance between ductile and brittle responses. The viscosity parameter was set to 1.16 to ensure numerical stability while avoiding excessive artificial damping; very low values (<0.1) caused convergence difficulties, whereas higher values (>2.0) distorted the load–displacement response. The parameter K_c=0.667 represents the default value in ABAQUS for concrete under multiaxial loading [35] sensitivity checks with K_c=0.75 confirmed minimal influence (<2% deviation in peak load). Poisson's ratio was set to 0.15, consistent with typical values for normal-strength concrete (ACI 318-19 [36]).

To verify robustness, sensitivity analyses were conducted by varying the CDP parameters within practical ranges. The dilation angle (Ψ) was examined at 20°, 30°, and 40°. The viscosity parameter (μ\muμ) was varied at 0.5, 1.16, and 2.0. The ratio of biaxial to uniaxial compressive strength (K_c) was checked at 0.667 and 0.75. Finally, Poisson's ratio (ν\nuν) was considered at 0.15 and 0.20. Other material and interface parameters such as concrete compressive strength, reinforcement yield strength, CFRP modulus and tensile strength, bolt pretension, anchorage length, and bond–slip parameters were also identified as potentially influential variables. While these were not systematically varied in the present study, their significance is acknowledged, and they will be the focus of future structured parametric or probabilistic sensitivity analyses.

The modulus of elasticity for concrete was determined using the ACI 318-19 [36] expression Eq .(1):

$$E_C = 4700\sqrt{f_c'}\ (MPa) \qquad (1)$$

(in FPS unit $E_C = 57000\sqrt{f_c'}\ (psi)$)

where E_c is the modulus of elasticity of concrete (MPa), and f_c' is the 28-day cylinder compressive strength of concrete (MPa).

Nonlinear uniaxial compressive behavior was described using the Kent and Park model (Fig. 3 and 4) [32,33], which defines the stress–strain relationship of unconfined concrete as shown in Eq .(2):

$$\sigma_C = f'_{co}\left[2\left(\frac{\varepsilon_c}{\varepsilon'_c}\right) - \left(\frac{\varepsilon_c}{\varepsilon'_c}\right)^2\right] \quad (2)$$

Where ε_c represents compressive strain, f'_{co} denotes the compressive strength of the unconfined cylindrical concrete specimen, and ε'_c a is the corresponding strain, assumed to be 0.002 [3,18,37,38]. Compressive stress iwas determined using Eq .(3) [18]:

$$\sigma_C = (1 - d_c)\, E_O\, (\varepsilon_C - \varepsilon_C{}^{\sim PL}) \quad (3)$$

$$\varepsilon_C{}^{\sim PL} = \left(\varepsilon_C{}^{\sim in} - \frac{1}{(1-d_c)}\frac{\sigma_c}{E_0}\right) \text{ and } dc = 1 - \frac{\sigma_c}{f'co} \quad (4)$$

In these Eq .(3) and Eq .(4), $\varepsilon_C{}^{\sim PL}$ represents inelastic strain, ε_C denotes compressive strain, E_O is the elasticity modulus, d_c is compressive damage, and $\varepsilon_C{}^{\sim \mathrm{in}}$ is the strain associated with damage [3,39–42].

$$dc = 1 - \frac{\sigma_c}{f'_{co}} \quad (5)$$

Where σ_C represents compressive stress and f'_{co} denotes the compressive strength of the unconfined cylindrical concrete specimen [3,39–42]. The constitutive behaviour of concrete was defined using the Kent–Park model in compression and the CEB-FIP formulation in tension. Since the experimental reference study did not provide full stress–strain curves, the ascending branch up to peak stress was based on the reported compressive strength and elastic modulus, while the post-peak softening branches were constructed according to Kent–Park (compression) and CEB-FIP (tension) recommendation. Table. 1 summarizes the adopted constitutive parameters for unconfined and confined concrete, and Figs. 3 and 4 illustrate the implemented stress–strain curves. For further details on the discretization procedure into ABAQUS CDP input, the reader is referred to our previous conference paper [43].

This model captures the influence of compressive damage on the unloading response, as shown in Fig. 4 [35]. The concrete stress-strain behavior in compression and the post-cracking tensile response were defined according to CEB-FIB guidelines [13]. Reinforcement was modelled with T3D2 truss elements embedded into the concrete domain using the embedded region constraint, which enforces a perfect bond assumption. Explicit bond–slip formulations for NSM bars have also been proposed in the literature [44,45]. These approaches reproduce local slip phenomena under monotonic and cyclic loading but require detailed experimental calibration. In this study, the embedded bond assumption was deemed sufficient given the absence of bond–slip failures in the reference experiments.

This simplification is widely adopted in RC joint modelling studies [3,18] and is appropriate in the present case, as the experimental reference did not report anchorage failure, lap splice slip, or NSM bar debonding. Therefore, the perfect bond assumption does not influence the global response or failure mechanism considered in this study. Reinforcement truss elements (T3D2) were ideal for capturing axial forces without bending stiffness, whereas CFRP sheets were represented with four-node shell elements (S4R), effectively modelling their thin-layer geometry and mechanical behaviour [3]. CFRP sheets were modelled using tie constraints, enforcing perfect adhesion with the concrete substrate. This simplification was adopted because the experimental benchmark did not exhibit FRP debonding; hence, interfacial failure was not part of the observed response. Since debonding behaviour was outside the scope of the present study, and the global performance (strength, ductility, energy dissipation) was the main focus, the tie assumption provided a reasonable and computationally efficient representation of the CFRP contribution.

Alternative approaches such as cohesive zone and bond–slip interface formulations have been widely adopted to capture FRP debonding [23,46]. These methods provide more accurate representation of interfacial fracture but require additional calibration. In the present study, tie constraints were adopted since no FRP debonding was reported in the benchmark tests

Concrete components were discretized with eight-node solid brick elements (C3D8R) to accurately simulate three-dimensional stress states, strain localization, and damage evolution [2]. Several mesh sizes were evaluated (15 mm, 20 mm, 25 mm, and 30 mm), and the results were compared in terms of peak load prediction, initial stiffness, and CPU time. Table. 2 summarizes the convergence results. It was observed that reducing the mesh size from 30 mm to 20 mm improved accuracy by more than 8% in peak load prediction, but further refinement to 15 mm resulted in less than 2% improvement while tripling the computational cost. The 25 mm mesh offered a balanced trade-off, with accuracy within 5% of the experimental results and a reasonable CPU time. Element aspect ratios were controlled to remain close to unity, particularly near reinforcement bars and CFRP–concrete interfaces, to avoid numerical locking or spurious stress concentrations. The adopted 25 mm element size has therefore been justified as an efficient and accurate choice, consistent with best practices in RC joint modelling (Fig. 5).

Careful consideration was given to interaction modeling among structural components. Reinforcement bars were embedded into concrete, utilizing the 'embedded' constraint to simulate a realistic and full-bond behavior between steel and concrete. CFRP sheets and concrete surfaces employed tie constraints to represent ideal adhesive bonds accurately. Steel plates used in external retrofitting techniques were modeled through surface-to-surface interactions with a defined friction coefficient of 0.3 to replicate realistic frictional behavior and potential slippage under seismic loads [18]. The same value has been widely adopted in previous studies on retrofitted RC joints [3], where $\mu \approx 0.3$ was shown to adequately represent steel–concrete interface behaviour under cyclic loading [47]. Advanced bolt and connector modeling strategies have also been reported [48], which explicitly simulate pretension and slip of fasteners. These were not implemented in the present work since bolt-level data were not available in the benchmark tests, and global plate–concrete interaction was adequately represented by frictional contact.

Boundary and loading conditions for the numerical models precisely mirrored experimental configurations. Columns were fixed at their ends, and displacement-controlled loading was imposed at the beam tip, reflecting quasi-static experimental loading protocols. Analyses were performed using the implicit static general solver in ABAQUS, capturing realistic quasi-static loading scenarios.

The reliability of numerical models was rigorously validated against experimental data (Fig. 6). Comparative analyses between numerical predictions and experimental observations, encompassing load-deflection responses, failure modes, and energy dissipation capacities, are comprehensively summarized in Table. 3. Numerical results consistently demonstrated close alignment with experimental outcomes, with deviations in maximum load capacity and observed failure modes maintained within 5%. This robust validation confirmed that the developed models effectively represent the complex seismic behavior of RC beam-column joints, thereby providing a solid foundation for subsequent parametric investigations and optimization of advanced retrofitting strategies. Although the numerical predictions showed excellent agreement with experimental data, minor deviations (within 5%) in the ultimate load capacity were observed. These small discrepancies are primarily attributed to idealized modeling assumptions, such as the perfect bond condition defined between CFRP and concrete surfaces using tie constraints and the inherent limitations of the CDP model in capturing localized discontinuities and micro-level damage progression. Detailed failure analysis indicated that numerical models effectively replicated shear cracking patterns in the joint regions; however, initiation and detailed propagation of CFRP debonding phenomena were slightly underestimated due to the assumption of ideal adhesion conditions. Regarding seismic performance, the models successfully reproduced critical response parameters such as ductility and energy dissipation capacity, which are vital for evaluating seismic resilience. Sensitivity analyses further highlighted the significant impact of variations in the dilation angle and friction coefficient parameters on post-peak response and failure mechanisms, underscoring the necessity of careful calibration of these parameters to enhance prediction accuracy. It should be emphasized that the validation in this study was performed against monotonic backbone curves extracted from cyclic tests. This approach is widely recognized in the literature when using the Concrete Damage Plasticity (CDP) model in ABAQUS, because the CDP formulation does not explicitly reproduce pinching and cyclic degradation. Therefore, validation against monotonic envelopes provides a reliable and computationally efficient benchmark for capturing peak load, stiffness, ductility indices, and failure modes, which are the critical parameters for comparative retrofit assessment in this study. Analyses were performed using the ABAQUS implicit static general solver with geometric nonlinearity enabled (NLGEOM=ON). The time increment was controlled with an initial value of 0.01, a minimum of 1.0×10^{-10}, and a maximum of 0.05 to ensure numerical stability. Convergence was monitored through force and displacement norms with a tolerance of 0.005. Concrete was discretized with linear 8-node brick elements (C3D8R) with enhanced hourglass control, while reinforcement and CFRP were modeled as described above. These solver controls and discretization settings have been explicitly reported to facilitate reproducibility of the numerical results.

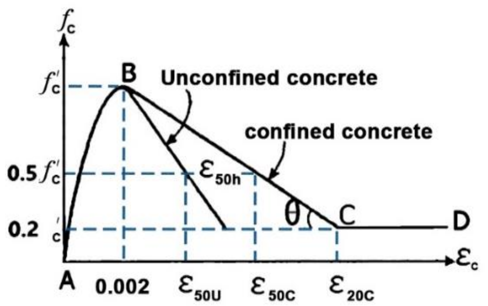

Fig.3: Comparison of stress–strain relationships for unconfined and confined concrete specimens. The unconfined curve represents the baseline response of plain concrete, while the confined curve illustrates the enhanced strength and ductility achieved through external confinement[49].

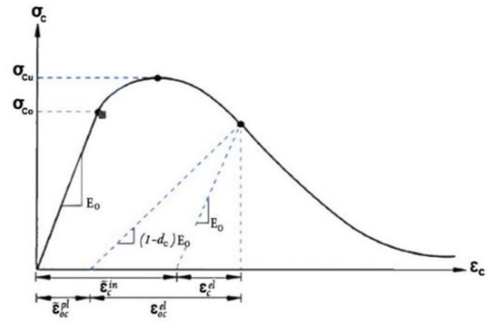

Fig. 4: Illustration of the impact of compressive damage on the unloading slope during the compression phase[50]. The figure highlights how progressive damage in concrete reduces the stiffness of the unloading branch, leading to a flatter slope compared with the initial elastic modulus.

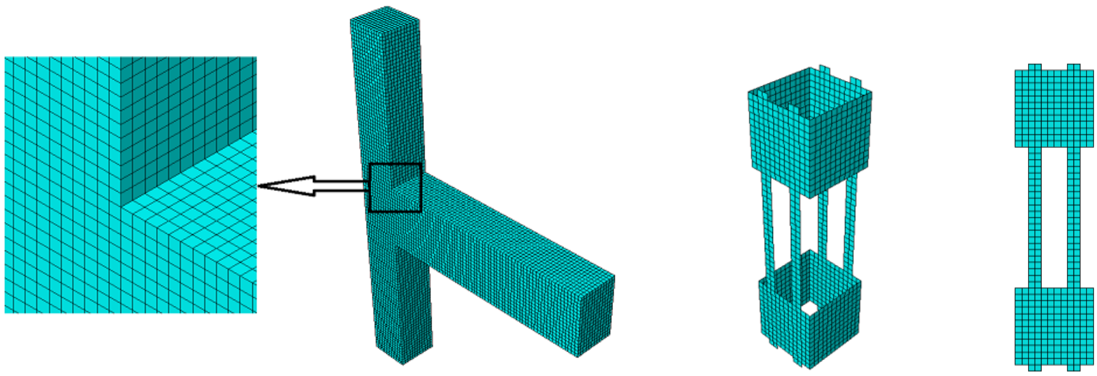

Fig. 5: Arrangement of FRP strips as depicted inand the mesh utilized in the verification model.

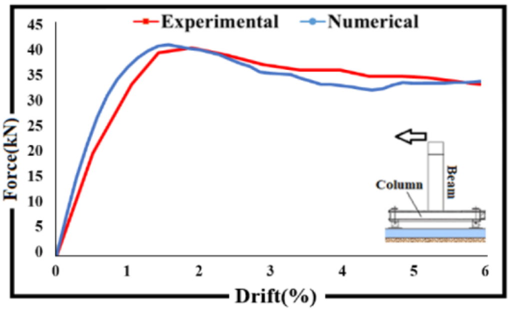

SJ0

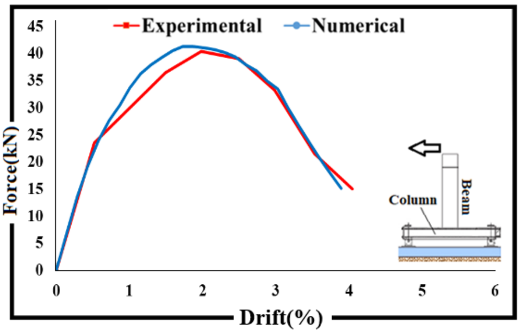

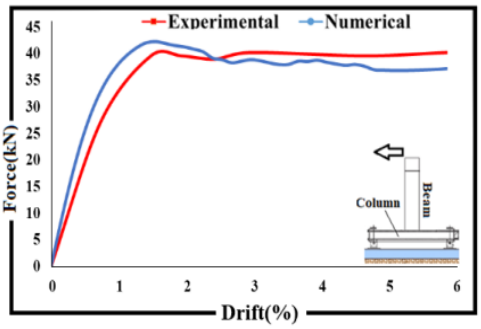

SJ3 RSJ3

(a)

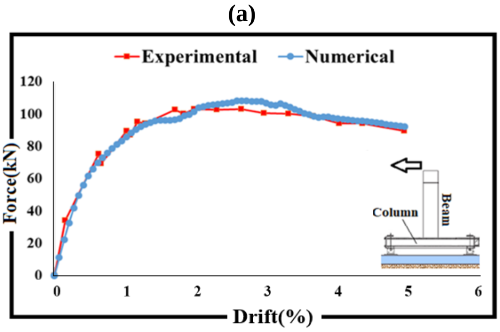

(b)

Fig. 6: Comparison between the force-displacement curve obtained from experimental results in and numerical analysis results. a) Khodaei et al. [11], b) Shrestha et al. [33].

Table 1: Adopted constitutive parameters for confined and unconfined concrete

State	f_c' (MPa)	E_c (MPa)	ε_{c0}	ε_{cu}	f_{ct} (MPa)	ε_{tu}	Notes
Unconfined	30.00	27.40	0.0020	0.0035	3.00	0.00015	Values from experimental ref. + CEB-FIP
Confined	36.00	29.00	0.0025	0.0060	3.50	0.00020	Calibrated using Kent–Park confinement

f_c': Cylinder compressive strength of concrete (taken from the experimental reference). E_c: Elastic modulus of concrete, calculated using the ACI expression ($Ec = 4700\sqrt{f_c'}$, MPa). εc0: Strain corresponding to peak compressive strength f_c' (≈0.002 for normal-strength concrete). εcu: Ultimate compressive strain in the descending branch; larger for confined concrete. f_{ct}: Tensile strength of concrete (approximately 10% of f_c' or estimated according to CEB-FIP). εtu: Ultimate tensile strain, typically very small (≈0.00015–0.00020). Notes: Short explanation about the source or calibration of the adopted values.

Table 2: Mesh convergence study

Mesh size (mm)	Peak load (kN)	Error vs. experiment (%)	CPU time (h)	Remarks
30	580	10.5	18	Coarse mesh
25	610	5.2	21	Balanced accuracy
20	620	3.6	28	Accurate, costly
15	625	2.1	33	High cost, minor gain

Table 3: Comparison of numerical and experimental results for validated specimens

Specimen	Numerical Maximum Load (kN)	Experimental Maximum Load (kN)	Deviation * (%)	Numerical Failure Mode	Experimental Failure Mode
SJ0	44.95	42.73	5.19	Flexural plastic hinge in beam	Flexural plastic hinge in beam
SJ3	41.25	39.42	4.65	Joint shear, rebar slip	Joint shear, rebar slip
RSJ3	43.21	41.52	4.07	Flexural hinge near retrofit, no joint shear	Flexural hinge near retrofit, no joint shear
Shrestha	105.52	102.73	2.72	joint shear cracks	joint shear cracks

*Deviation calculated as [(Numerical – Experimental)/Experimental] × 100.

4 . Specimens Under Investigation

In this study, seven advanced finite element models were developed to systematically investigate the seismic performance of RC beam-column joints and to evaluate the relative effectiveness of various retrofitting strategies. The ductile (D) specimen (Fig. 7a) serves as the reference model and represents a well-detailed, code-compliant joint, incorporating all modern seismic requirements such as adequate transverse reinforcement, proper anchorage of longitudinal bars, and closely spaced stirrups. This configuration ensures ductile flexural response and provides the benchmark for optimal seismic performance.

In contrast, the non-ductile (N.D) specimen (Fig. 7b) simulates a deficient joint typical of pre-1970s construction, characterized by the absence of joint core stirrups, inadequate bar anchorage, and increased stirrup spacing. This results in a brittle, shear-dominated failure mode and serves as the baseline for all retrofit scenarios, reflecting common vulnerabilities in existing RC frames of seismic regions.

A range of targeted retrofitting techniques were applied to the N.D specimen, each selected based on their effectiveness in addressing specific deficiencies and their proven applicability in practice: Bolt Steel Angle Cage (BSAC, Fig. 7c): External L-shaped steel angles (L 80×80×8 mm), anchored by high-strength M16 bolts, provide robust confinement and significantly enhance both shear and flexural capacity. This method was selected for its straightforward installation and substantial improvement in joint integrity. Bolted Steel Box (BSB, Fig. 7d): Steel box sections (40×80×4 mm), positioned on either side of the beam and fixed with bolts to a rear box plate, act as external tensile reinforcement and efficiently increase joint lateral strength. BSB is especially effective for rapid, geometry-preserving strengthening. Externally Bonded CFRP (CFRP, Fig. 7e): Carbon fiber sheets, arranged diagonally (X-shape) over the joint core and as U-shaped strips on the beam and column faces, offer a lightweight, corrosion-resistant solution that markedly improves energy dissipation and ductility. Hybrid CFRP-BSB Configuration (Fig. 7f): The combination of the BSB system with diagonal CFRP strips is intended to leverage the strengths of both steel and fiber reinforcement, aiming for maximum strength and ductility.

CFRP-NSM Hybrid (Fig. 7g): This approach integrates externally bonded CFRP with near-surface mounted (NSM) high-strength steel bars, which are embedded in grooves near the beam surface and anchored into the column. This combination compensates for inadequate bar anchorage and simultaneously enhances both flexural and shear performance. The detailed geometry, reinforcement layout, and retrofitting arrangements for all specimens are shown in Figures 7a–7g. By selecting these retrofit schemes, a comprehensive range of modern strengthening philosophies is covered—including steel-based, FRP-based, and hybrid systems—each with its unique balance of constructability, weight, corrosion resistance, and seismic performance. Steel-based solutions provide robust confinement but add structural weight and may increase corrosion risk. FRP-based retrofits are lightweight and highly effective in energy dissipation, though they require precise surface preparation. Hybrid approaches seek to combine these advantages for optimized performance.

This systematic modeling framework enables a robust comparative assessment of all retrofit strategies in terms of strength, stiffness, ductility, and energy dissipation, as discussed in the following sections (see Figs. 7a–7g). The insights gained here offer practical guidance for selecting and applying the most suitable retrofit method for vulnerable RC structures in seismic zones.

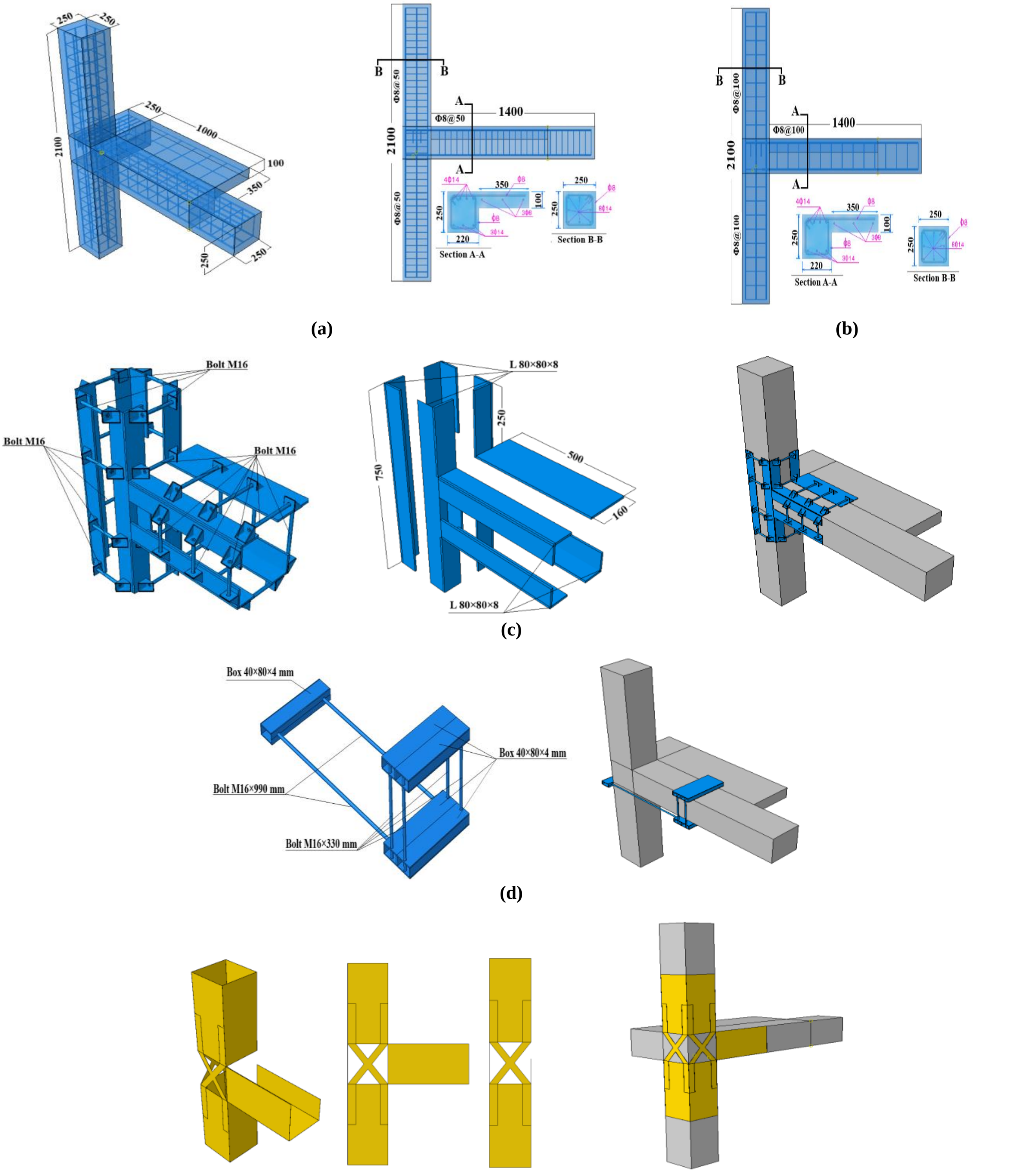

(a)

(b)

(c)

(d)

(e)

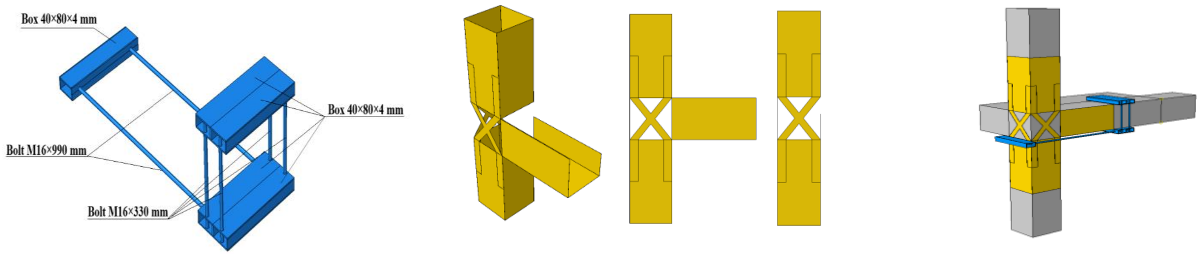

(f)

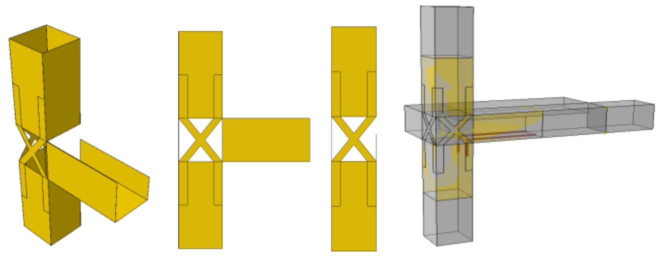

(g)

Fig 7: Schematic illustration of all finite element specimens investigated: (A) Ductile (D), (B) Non-ductile (N.D), (C) Bolt Steel Angle Cage (BSAC), (D) Bolted Steel Box (BSB), (E) Carbon Fiber Reinforced Polymer (CFRP), (F) Hybrid CFRP-BSB, and (G) CFRP with Near Surface Mounted bars (CFRP-NSM).

4.1 Investigation of Monotonic Force-Displacement Curves

Fig. 8 illustrates the monotonic force–displacement curves for all investigated specimens, with each model compared directly to the non-ductile (N.D) joint under identical loading and boundary conditions. Table. 4 presents a comprehensive summary of the key numerical parameters for each specimen, including cracking load and displacement (V_{cr}, Δ_{cr}), yield load and displacement (V_y, Δ_y), peak and ultimate load (V_p, V_u), and their corresponding displacements (Δ_p, Δ_u).

The ductile (D) specimen, representing a well-detailed joint, serves as the benchmark for optimal seismic performance. As shown in Fig. 8a, the D specimen exhibits the highest initial stiffness and achieves a peak load of 43.05 kN and an ultimate displacement of 84 mm—significantly surpassing the N.D joint, which reaches only 41.25 kN and 42.38 mm, respectively. The D specimen demonstrates stable post-peak behavior, gradual strength degradation, and superior energy dissipation, underscoring the effectiveness of code-compliant detailing in enhancing both strength and ductility.

Retrofitted specimens show considerable improvement over the N.D control in every critical aspect. The BSAC configuration (Fig. 8b), utilizing an external steel angle cage, increases the peak load to 53.63 kN and ultimate displacement to 84 mm, nearly doubling the deformation capacity compared to the N.D joint. The BSB system (Fig. 8c), featuring bolted steel boxes, achieves a similar enhancement, with notable improvements in both strength and displacement due to the effective confinement provided by the steel assembly.

Application of externally bonded CFRP sheets (Fig. 8d) further elevates the joint's response, achieving a peak load of 59.85 kN and maintaining strength across the full displacement range. The unique cross and U-shaped fiber arrangement ensures a balanced improvement in both flexural and shear behavior, resulting in higher ductility and a more controlled post-peak softening.

The most significant gains are observed in the hybrid systems. The CFRP-BSB specimen (Fig. 8e), which combines the BSB retrofitting system with diagonal CFRP strengthening, leverages the synergistic effects of mechanical and composite confinement, achieving a peak load of 59.97 kN and an ultimate displacement of 84 mm. The CFRP-NSM configuration (Fig. 8f), integrating near-surface mounted steel bars with CFRP wrapping, delivers the highest peak load (64.17 kN) and displays the most ductile response among all specimens, with a stable plateau and delayed strength degradation after peak.

Collectively, the monotonic force–displacement curves reveal a clear trend: all advanced retrofitting strategies substantially improve both strength and deformation capacity of deficient RC beam-column joints. Hybrid methods, particularly those combining steel and CFRP (CFRP-BSB and CFRP-NSM), demonstrate the greatest enhancements in peak strength, ultimate displacement, and post-peak stability, often exceeding the performance of the ductile reference specimen. These findings, comprehensively presented in Table. 4 and Fig. 8, highlight the critical role of tailored retrofit solutions in upgrading vulnerable RC joints for seismic resilience and ensure that structural safety and ductility demands are met in existing infrastructure.

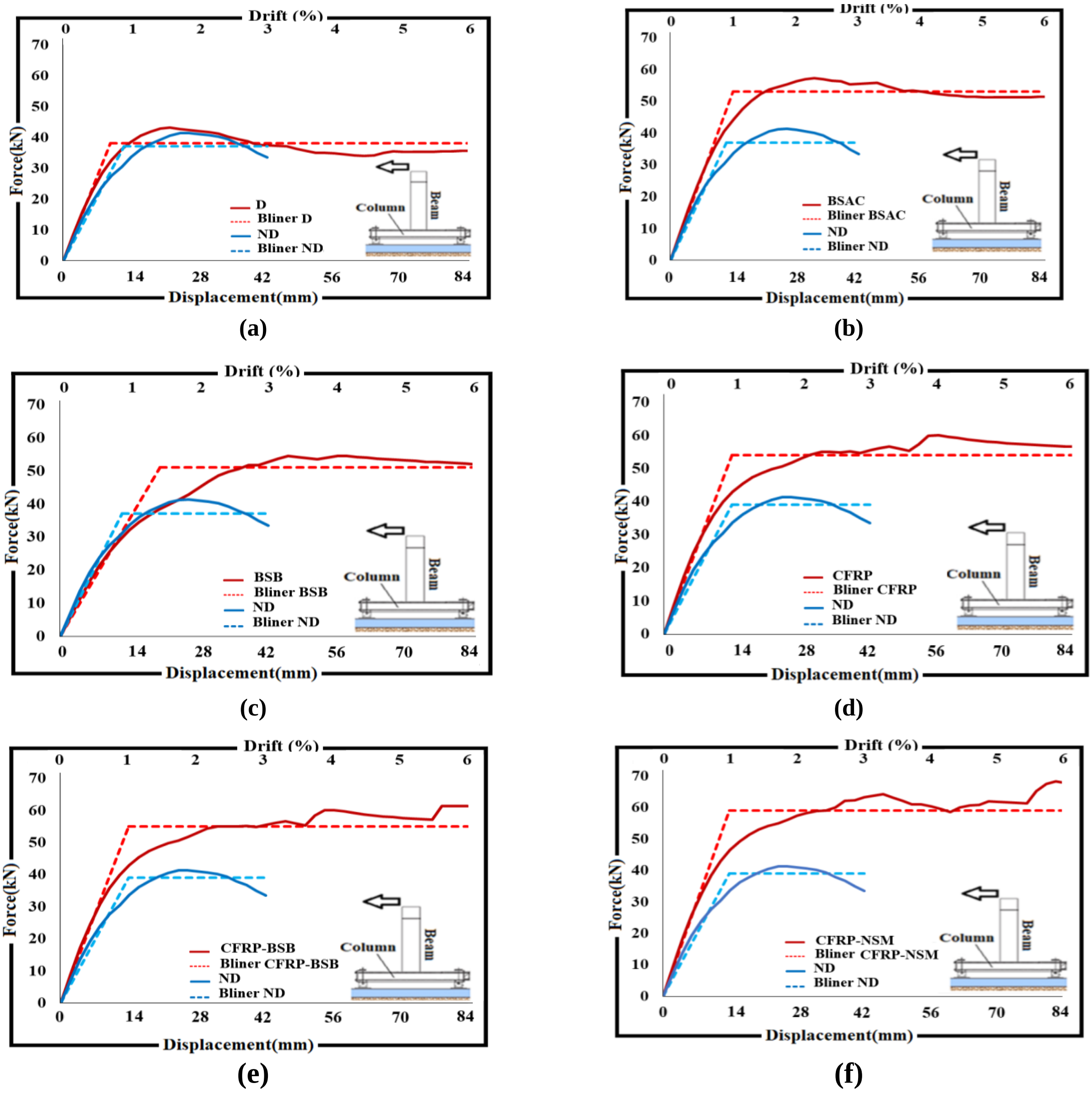

Fig 8: Monotonic force–displacement curves for all retrofitted specimens compared to the non-ductile (N.D) joint: (a) N vs. N.D (b) BSAC vs. N.D, (c) BSB vs. N.D, (d) CFRP vs. N.D, (e) CFRP-BSB vs. N.D, (f) CFRP-NSM vs. N.D.

Table 4: Summary of load and displacement parameters for all investigated specimens.

Specimen	V_{cr} (kN)	Δ_{cr} (mm)	V_y (kN)	Δ_y (mm)	V_p (kN)	Δ_p (mm)	V_u (kN)	Δ_u (mm)
D	15.96	4.03	32.68	10.09	43.05	22.20	35.58	84.00
N.D	13.51	4.03	27.56	10.09	41.25	26.23	33.37	42.38
BSAC	16.11	4.03	35.76	10.09	57.25	32.29	51.36	84.00
BSB	11.27	4.03	29.05	12.11	53.63	44.04	51.99	84.00
CFRP	17.10	4.03	39.76	12.11	59.85	54.49	56.60	84.00
CFRP-BSB	17.11	4.03	39.77	12.11	59.97	54.49	57.01	84.00
CFRP-NSM	17.96	4.03	42.80	12.11	64.17	46.42	61.28	84.00

4.2 Investigation of ductility ratio

Ductility refers to the capacity of a structural system to sustain substantial inelastic displacements while maintaining an acceptable decrease in its load-carrying capacity. This is quantified by the structure's overall ductility ratio (μ), which is derived from the idealization of its performance curve into equivalent bilinear curves representing elastic and perfectly plastic behavior. According to Eq .(6), μ is calculated by dividing the maximum relative lateral displacement (du) by the relative yield lateral displacement (dy) [4,43,49]. In specimens under consideration, relative lateral displacement is equal to deflection of beam end.

$$\mu = \frac{d_u}{d_y} \quad (6)$$

The displacement corresponding to a fraction of the peak load (Fp) can be considered the ultimate point. According to literature, this fraction typically ranges between 10% and 20% [37,42,43]. Fig. 9 illustrates an equivalent ideal bilinear diagram used to assess the ductility ratio. The results for all specimens are summarized in Table. 5. The procedure for determining the characteristic displacements was as follows: the cracking displacement (Δcr) was identified as the first deviation from linearity in the load–displacement curve. Because the initial elastic stiffness and material properties (concrete and reinforcement) were identical across all models prior to retrofit intervention, Δcr occurred consistently at 4.03 mm for all specimens. The yield displacement (Δy) was determined using the bilinear idealization method, based on the intersection of the initial elastic slope with the horizontal yield load line. As a result, specimens sharing the same initial stiffness exhibited identical Δy values (e.g., Δy = 10.09 mm for D and BSAC). The ultimate displacement (Δu) was defined at the point where the lateral load decreased to 80% of the peak load (Vu = 0.8Vp), in accordance with Eq. (6). Consequently, the ductility ratios (μ) for several retrofitted specimens were identical (e.g., μ = 6.94), reflecting similar backbone responses under the adopted criteria. These repetitions are therefore a direct outcome of the consistent calculation method rather than reporting artifacts. The ductile (D) specimen and the BSAC-retrofitted joint both achieved the highest ductility ratio (μ = 8.32), reflecting a 98.2% increase compared to the non-ductile (N.D) control joint (μ = 4.20). This exceptional improvement for BSAC can be directly attributed to the continuous external confinement provided by the steel angle cage, which delays the formation of critical shear cracks and effectively restrains joint degradation. All other advanced retrofitting systems—including BSB, CFRP, CFRP-BSB, and CFRP-NSM—demonstrated a consistent and substantial enhancement in ductility (μ = 6.94), corresponding to a 65.15% increase over the N.D joint. The improvement observed with these methods is the result of effective confinement and redistribution of stresses within the joint region, achieved through the combined action of external steel or fiber reinforcement and, in hybrid systems, the synergy between mechanical and composite strengthening mechanisms. It is noteworthy that the addition of near-surface mounted (NSM) bars to the CFRP wrapping did not result in further increases in ductility compared to the other CFRP or BSB configurations. This suggests that, while NSM bars are effective in enhancing strength and post-yield stiffness, their contribution to deformation capacity may be governed by the overall joint configuration or the governing failure mode.

All retrofitted specimens, regardless of the method employed, successfully reached the maximum drift limit of 6%, indicating robust deformation capacity and reliable delay of brittle failure. From a seismic design perspective, these ductility enhancements are critical: higher ductility ratios not only increase the ability of a joint to dissipate seismic energy but also significantly reduce the likelihood of sudden, catastrophic failure—a key requirement in modern performance-based earthquake engineering. Collectively, these findings confirm that tailored retrofitting solutions can restore or even surpass the ductility of modern code-compliant joints in deficient RC frames. The data provide quantitative and qualitative benchmarks for selecting the most suitable retrofit strategies in practical seismic rehabilitation applications.

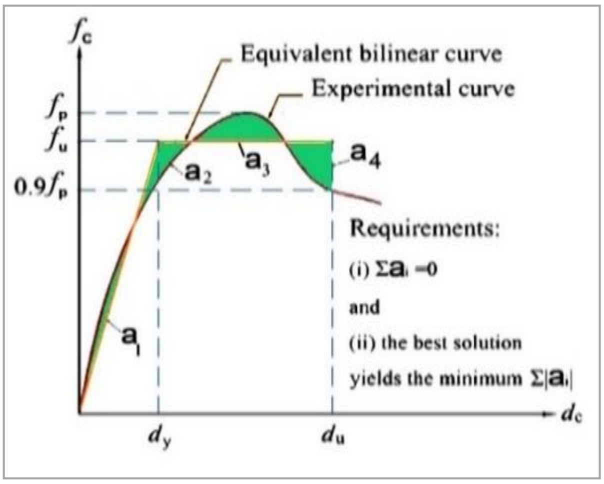

Fig. 9: Equivalent bilinear curve definition for ductility ratio evaluation[18]

Table 5: Ductility ratio and related factors in retrofitted and base specimens

Specimen	dy (Dic)&(Drift) (mm)	Du (Dic)&(Drift) (mm)	$\mu = \frac{d_u}{d_y}$	Increase of ductility ratio (%)
D	10.09	84.00	8.32	98.20
N.D	10.09	42.38	4.20	-
BSAC	10.09	84.00	8.32	98.20
BSB	12.11	84.00	6.94	65.15
CFRP	12.11	84.00	6.94	65.15
CFRP-BSB	12.11	84.00	6.94	65.15
CFRP-NSM	12.11	84.00	6.94	65.15

4.3 The maximum plastic strain index

In this study, the plastic strain index (PE) refers to the maximum principal plastic strain output variable (PE) available in ABAQUS under the Concrete Damage Plasticity (CDP) model. This index is dimensionless and quantifies the accumulated inelastic strain beyond the elastic limit. For each specimen, PE values were extracted at all integration points, and the maximum value within the joint core was reported as the global indicator of damage severity. The spatial distribution and maximum values of the principal plastic strain index (PE) for all specimens are presented in Fig. 10a–g, with corresponding quantitative data summarized in Table .6. This index provides critical insight into the localization and extent of inelastic damage in the joint region, thereby serving as a sensitive indicator for the evaluation of different retrofitting strategies under seismic demands [18]. According to established literature (e.g., Kent & Park, 1971; Vecchio & Collins, 1986), PE values on the order of 10^{-2} to 10^{-1} correspond to distributed and acceptable damage levels, while values exceeding ~1.0×10^{-1} typically indicate excessive strain localization and potential crushing or spalling. These thresholds provide an objective reference for interpreting the numerical results in Table. 6 and Fig10.

The ductile reference specimen (Fig. 10a) displayed a maximum PE of 9.135×10^{-2}, with plastic strains well-distributed throughout the joint core. This widespread, yet controlled, distribution underscores the effectiveness of code-compliant reinforcement detailing in facilitating energy dissipation and delaying the onset of severe localized damage. In sharp contrast, the non-ductile (N.D) specimen (Fig. 10b) exhibited a similar but slightly lower maximum PE (8.025×10^{-2}); however, the concentration of high plastic strain in limited regions reflects the heightened vulnerability to brittle failure in the absence of adequate confinement.

Among the retrofitted specimens, the BSAC system (Fig. 10c) achieved a maximum PE of 8.318×10^{-2}, closely matching the ductile benchmark and confirming that robust external steel cage confinement can restore both the magnitude and spatial distribution of plastic strains to those of a modern, well-detailed joint. Conversely, the BSB configuration (Fig. 10d) exhibited a notably higher maximum PE of 5.872×10^{-1}—an order of magnitude greater than other systems—indicating severe localized inelastic demand and suggesting potential for premature local crushing or spalling despite improvements in overall load capacity.

To elaborate, the dramatically higher PE observed in the BSB specimen compared with all other systems (~0.08–0.09) highlights a fundamental drawback of this retrofit method. The sharp box corners act as rigid “hard points,” generating concentrated stress paths that drive localized inelastic deformation. In addition, the bolted connection system may induce secondary pinching and prying actions at the steel–concrete interface, which exacerbate strain localization and accelerate the onset of crushing or spalling. These mechanisms collectively explain the anomalous PE response and clearly differentiate the BSB system from other retrofitting techniques. From a design perspective, this indicates that while BSB increases global strength, it may simultaneously compromise ductility and damage tolerance unless additional measures—such as rounded geometry, distributed anchorage, or hybrid overlays with CFRP—are incorporated to mitigate stress concentration effects.

This anomalously high PE can be attributed to the geometry of the steel box retrofit, which creates rigid boundary zones at the corners of the joint. These act as “hard points,” concentrating stresses and forcing inelastic strains into narrow regions of the joint core. In addition, the bolted connection may introduce localized pinching or prying actions at the steel–concrete interface, further exacerbating strain localization. Together, these mechanisms explain why the BSB system, despite enhancing global load capacity, generates unfavorable strain concentration and potential for premature crushing or spalling.

The externally bonded CFRP specimen (Fig. 10e) recorded a maximum PE of 7.865×10^{-2}, demonstrating the ability of carbon fiber reinforcement to suppress excessive plasticity and promote more favorable, distributed damage patterns within the joint. This benefit is even more pronounced in the hybrid CFRP-BSB configuration (Fig. 10f), where the maximum PE was further reduced to 7.524×10^{-2}. The combination of mechanical and composite confinement proved particularly effective in mitigating the concentration of plastic strains and thus enhancing damage control and ductility. Finally, the CFRP-NSM hybrid specimen (Fig. 10g) reached a maximum PE of 8.736×10^{-2}, reflecting a balanced performance that closely approximates that of the ductile and BSAC specimens. The integration of near-surface mounted steel bars with CFRP wrapping provided effective synergistic enhancement of both strength and damage tolerance. Collectively, the results depicted in Figure 10 and summarized in Table. 6 reveal that advanced retrofitting schemes—especially those utilizing hybrid steel-FRP strategies or CFRP-only solutions—are most effective in reducing the intensity and localization of inelastic damage within RC beam-column joints. By contrast, systems relying solely on external steel boxes (BSB) may be prone to undesirable strain concentration and localized damage, highlighting the importance of composite or hybrid confinement in ensuring reliable seismic resilience. These findings underscore the utility of the maximum plastic strain index as a robust comparative metric and provide a quantitative foundation for the selection and optimization of retrofit strategies in the seismic strengthening of existing RC structures.

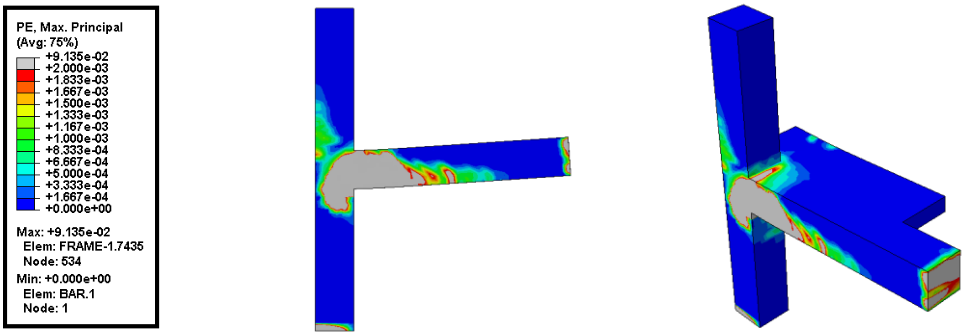
PE, Max. Principal
(Avg: 75%)
+9.135e-02
+2.000e-03
+1.833e-03
+1.667e-03
+1.500e-03
+1.333e-03
+1.167e-03
+1.000e-03
+8.333e-04
+6.667e-04
+5.000e-04
+3.333e-04
+1.667e-04
+0.000e+00
Max: +9.135e-02
Elem: FRAME-1.7435
Node: 534
Min: +0.000e+00
Elem: BAR.1
Node: 1

(a)

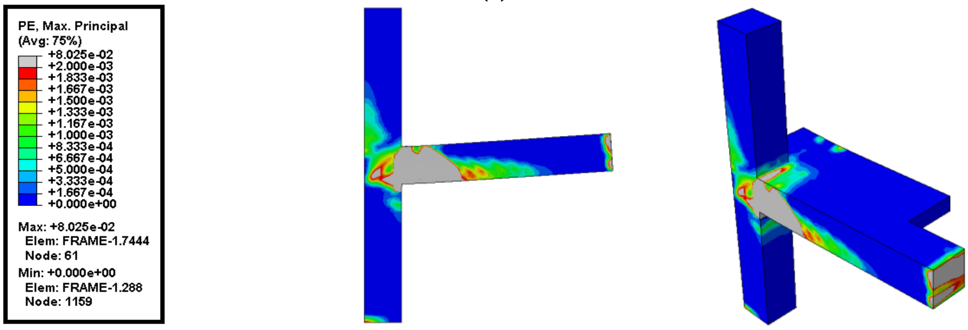
PE, Max. Principal
(Avg: 75%)
+8.025e-02
+2.000e-03
+1.833e-03
+1.667e-03
+1.500e-03
+1.333e-03
+1.167e-03
+1.000e-03
+8.333e-04
+6.667e-04
+5.000e-04
+3.333e-04
+1.667e-04
+0.000e+00
Max: +8.025e-02
Elem: FRAME-1.7444
Node: 61
Min: +0.000e+00
Elem: FRAME-1.288
Node: 1159

(b)

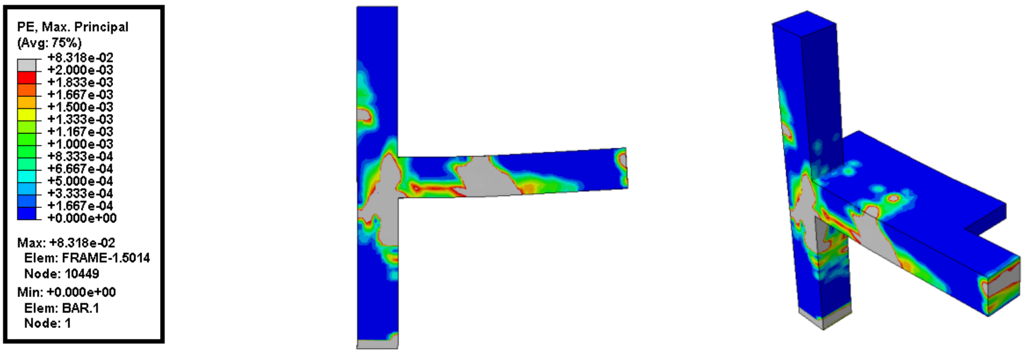
PE, Max. Principal
(Avg: 75%)
+8.318e-02
+2.000e-03
+1.833e-03
+1.667e-03
+1.500e-03
+1.333e-03
+1.167e-03
+1.000e-03
+8.333e-04
+6.667e-04
+5.000e-04
+3.333e-04
+1.667e-04
+0.000e+00
Max: +8.318e-02
Elem: FRAME-1.5014
Node: 10449
Min: +0.000e+00
Elem: BAR.1
Node: 1

(c)

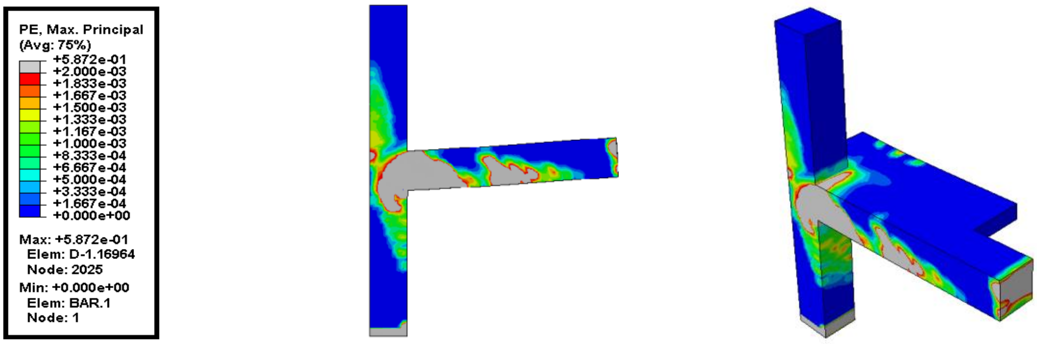
PE, Max. Principal
(Avg: 75%)
+5.872e-01
+2.000e-03
+1.833e-03
+1.667e-03
+1.500e-03
+1.333e-03
+1.167e-03
+1.000e-03
+8.333e-04
+6.667e-04
+5.000e-04
+3.333e-04
+1.667e-04
+0.000e+00
Max: +5.872e-01
Elem: D-1.16964
Node: 2025
Min: +0.000e+00
Elem: BAR.1
Node: 1

(d)

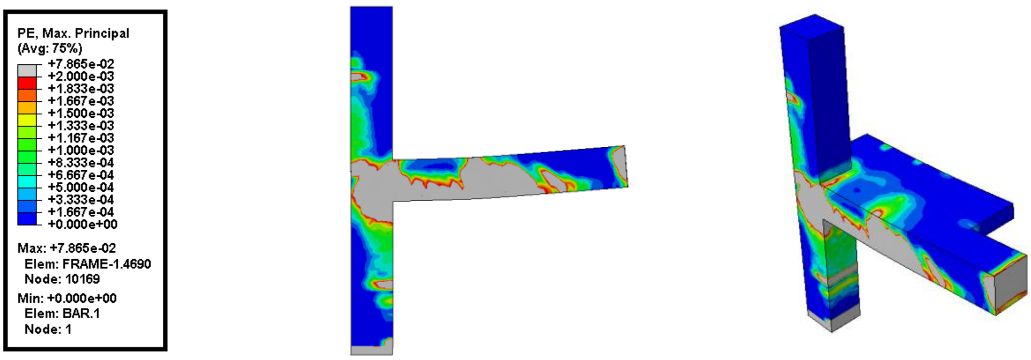
PE, Max. Principal
(Avg: 75%)
+7.865e-02
+2.000e-03
+1.833e-03
+1.667e-03
+1.500e-03
+1.333e-03
+1.167e-03
+1.000e-03
+8.333e-04
+6.667e-04
+5.000e-04
+3.333e-04
+1.667e-04
+0.000e+00
Max: +7.865e-02
Elem: FRAME-1.4690
Node: 10169
Min: +0.000e+00
Elem: BAR.1
Node: 1

(e)

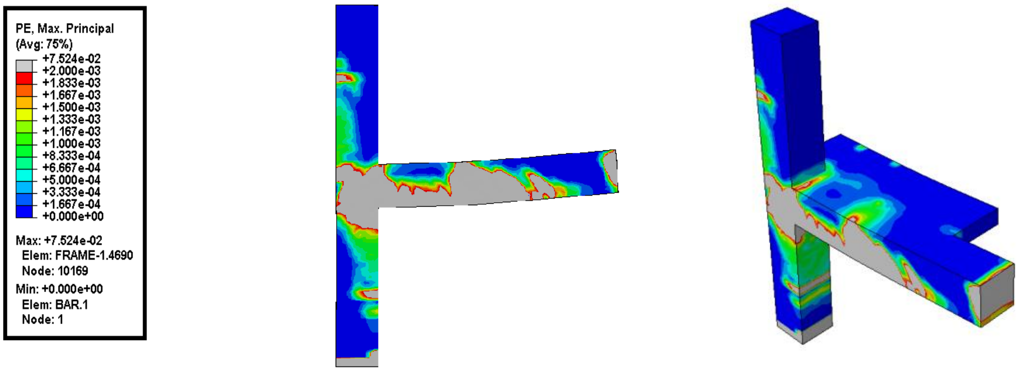

(f)

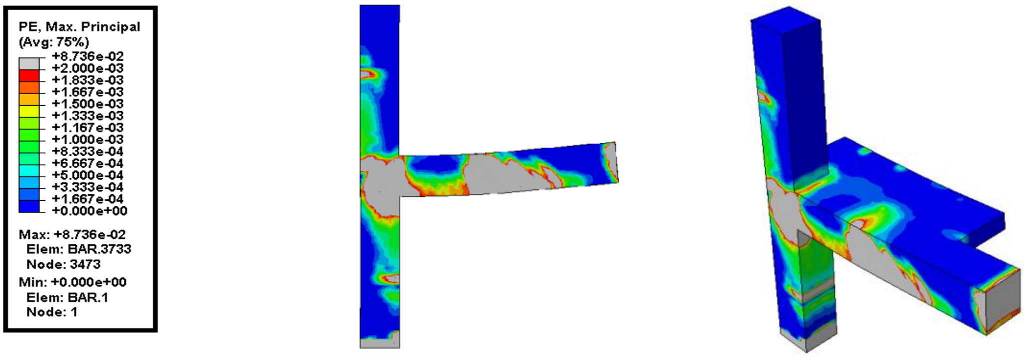

(g)

Fig. 10: Maximum Principal Plastic Strain Contours for RC Beam-Column Joint Specimens under Monotonic Loading

Table 6: Maximum plastic strain index (PE) for all specimens

Specimen	Maximum PE ($\times10^{-2}$)	Interpretation
Ductile (D)	9.135×10^{-2}	Acceptable distributed damage
Non-ductile (N.D)	8.025×10^{-2}	Localized damage – brittle-prone
BSAC	8.318×10^{-2}	Controlled, similar to D
BSB	5.872×10^{-1}	Excessive localized damage
CFRP	7.865×10^{-2}	Acceptable distributed damage
CFRP-BSB	7.524×10^{-2}	Controlled, hybrid effective
CFRP-NSM	8.736×10^{-2}	Acceptable distributed damage

5. Discussion and Practical Implications

The comparative evaluation of retrofitting strategies presented in this study highlights critical trends in both the mechanical response and damage control capacity of RC beam-column joints. The numerical results indicate that advanced retrofitting solutions—particularly those utilizing hybrid approaches that combine external steel confinement and fiber-reinforced polymers—consistently deliver superior improvements in strength, ductility, and damage mitigation compared to conventional methods or unretrofitted specimens. The BSAC and CFRP-BSB systems, in particular, demonstrated the ability to restore ductility and damage control performance to levels on par with or even exceeding those of modern code-compliant joints. This can be attributed to the synergy between mechanical confinement and the crack-bridging effect of composite materials, which effectively restrict the progression of inelastic deformations and prevent premature brittle failure. Notably, the CFRP-only and CFRP-NSM retrofits also provided substantial gains in ductility and plastic strain control, coupled with the practical advantages of lightweight application and corrosion resistance. Conversely, while the BSB retrofit improved joint strength and deformation capacity, the high concentration of plastic strains observed in this system underscores the importance of carefully designing steel-concrete interfaces and optimizing anchorage details to avoid localized damage. The observed increase in PE is consistent with stress concentration effects caused by the box geometry and possible prying at bolted connections. This behavior highlights a fundamental limitation of the BSB retrofit. Although the system is structurally efficient in increasing joint strength, the geometry of the steel box inherently produces hard-point effects at the corners, while the bolted anchorage may induce local prying and pinching. These mechanisms together cause severe strain localization, as evidenced by the maximum PE value (0.587) being nearly an order of magnitude higher than all other specimens (~0.08–0.09). Such a response clearly indicates that, without additional detailing measures, the BSB system may unintentionally compromise ductility and damage tolerance despite providing strength gains. Designers should therefore interpret the BSB results with caution and consider modifications such as rounded edges, distributed anchorage, or hybridization with CFRP to achieve balanced seismic performance. For designers, this suggests that unless anchorage and load transfer details are optimized, BSB systems may unintentionally sacrifice ductility and damage tolerance in favor of higher strength. This trade-off highlights the need for more refined detailing (e.g., rounded corners, distributed anchorage, or composite overlays) to mitigate hard-point effects and ensure balanced seismic performance. These findings suggest that the indiscriminate application of external steel elements without consideration of stress redistribution can be detrimental to long-term performance. From a practical perspective, the outcomes of this study provide a robust quantitative foundation for selecting retrofitting techniques tailored to specific performance objectives and site constraints. Hybrid strategies that integrate mechanical and composite confinement offer the most reliable path to seismic resilience, balancing constructability, efficiency, and durability. It should be noted, however, that these conclusions are based on monotonic analyses. While monotonic simulations are widely adopted as a first-order benchmark in CDP-based finite element modeling, they do not explicitly capture cyclic degradation, low-cycle fatigue, or unloading/reloading stiffness deterioration. Accordingly, the reported improvements in "seismic resilience" should be interpreted in a comparative sense—referring to enhanced strength, ductility, and plastic strain indices under monotonic conditions—rather than full equivalence to cyclic or dynamic seismic performance. Further cyclic or dynamic analyses are recommended to confirm these comparative findings. Moreover, the results emphasize the necessity of comprehensive damage assessment—including indices such as PE—in addition to traditional strength and stiffness metrics, to ensure that retrofitted joints achieve the desired level of safety under earthquake loading. Finally, the insights gained here are directly transferable to the seismic rehabilitation of deficient RC structures in regions with similar construction practices and hazard profiles. The proposed modeling approach and validation framework also serve as a basis for further research, encouraging the integration of experimental and numerical investigations to refine retrofit design guidelines and advance earthquake-resistant engineering practice. Beyond structural performance, practical feasibility and constructability are critical determinants in selecting retrofit strategies. Table. 7 provides a comparative summary of constructability and practical aspects of the investigated retrofitting schemes. As shown, CFRP-based retrofits (EBR) offer clear advantages in terms of rapid installation, minimal occupancy disruption, and reduced site preparation, albeit at a moderate material cost. NSM schemes require additional groove cutting, which increases time and complexity compared to externally bonded CFRP, while hybrid CFRP–steel systems combine the disadvantages of both methods. Steel-only systems (BSB, BSAC), although structurally effective, generally involve higher cost, longer installation time, and greater disruption due to welding and anchorage requirements. These comparative insights provide a more quantitative basis for evaluating constructability and practical .feasibility in addition to structural performance.

Table 7: Comparative assessment of practical and constructability aspects of retrofit techniques.

Retrofit scheme	Relative cost	Installation time	Occupancy impact	Site preparation required	Installation difficulty
BSB (steel box)	High	Long	Full disruption	Welding, surface prep	Difficult
BSAC (steel angle cage)	Medium–High	Medium	Partial disruption	Welding, anchorage	Moderate
CFRP (EBR)	Medium	Short	Minimal	Surface cleaning only	Easy
CFRP–NSM	Medium–High	Medium	Partial	Groove cutting + bonding	Moderate
CFRP–BSB (hybrid)	High	Long	Full	Welding + surface bonding	Difficult

5.1 Limitations and Recommendations for Future Research

A key limitation of this study is that validation was restricted to monotonic backbone responses rather than full cyclic hysteresis loops. Consequently, cyclic phenomena such as pinching, stiffness degradation, and cumulative energy dissipation were not explicitly captured. This limitation is inherent to the ABAQUS CDP model, which is widely known to reproduce monotonic envelopes more reliably than cyclic pinching behaviour. Future research will incorporate explicit cyclic loading protocols to address this gap. Despite the comprehensive nature of this numerical investigation, several limitations should be acknowledged. The finite element models were calibrated and validated primarily against monotonic loading scenarios; as such, the cyclic degradation, cumulative damage, and low-cycle fatigue effects characteristic of seismic actions were not explicitly captured. It should also be noted that the reported ductility indices are sensitive to the adopted yield and ultimate definitions. As a result, some values (e.g., $\Delta cr = 4.03$ mm or $\mu = 6.94$) appear repeatedly across different specimens. These repetitions arise naturally from the consistent bilinear idealization criteria and common initial stiffness of the models, rather than from reporting or algorithmic errors.

The idealized modeling assumptions—such as perfect bond conditions between concrete and reinforcement or CFRP, and the adoption of a constant friction coefficient ($\mu = 0.3$) for steel–concrete interfaces—may not fully represent the complexities of real-world construction. While $\mu = 0.3$ is consistent with standard practice in retrofit modeling, it does not capture potential variations arising from surface roughness, bolt pre-load, or degradation effects, which may significantly influence interface behavior over time. While $\mu = 0.3$ is consistent with standard practice in retrofit modeling, it does not capture potential variations due to surface roughness, bolt preload, or degradation effects, which may significantly influence interface behavior over time. Another limitation is that the sensitivity analyses were restricted to selected CDP and interface parameters (dilation angle and friction coefficient). Important practical variables such as concrete strength, steel yield stress, CFRP property scatter, bolt pretension, anchorage length, and bond parameters were not explicitly examined. Future research should incorporate structured parametric or probabilistic sensitivity studies on these variables to establish the robustness of retrofit performance under realistic material and construction uncertainties. Furthermore, the absence of full-scale experimental validation for some hybrid retrofitting configurations introduces additional uncertainty regarding long-term performance and constructability. Future research should address these gaps by incorporating cyclic and dynamic loading protocols, detailed bond-slip and interface models, and systematic experimental campaigns on retrofitted joints with realistic construction defects and aging effects. Life-cycle cost analysis, field application challenges, and optimization of retrofit detailing should also be explored to facilitate the practical adoption of advanced hybrid and composite retrofitting techniques in seismic rehabilitation projects.

6. Conclusions

This study has presented a comprehensive numerical investigation into the behavior and retrofitting of deficient RC beam-column joints using a range of advanced strengthening techniques. The validated finite element models, calibrated against experimental benchmarks, enabled a detailed assessment of both conventional and innovative retrofitting schemes under monotonic loading conditions. The results demonstrate that all retrofitting approaches examined—especially hybrid systems combining external steel cages or boxes with fiber-reinforced polymer (FRP) composites—significantly enhance the monotonic strength, ductility, and damage control capacity of non-ductile joints. Among these, the BSAC and CFRP-BSB systems restored ductility and damage control performance to levels comparable with or in some cases approaching those of code-compliant ductile specimens under monotonic loading conditions, achieving an optimal balance between mechanical strength and controlled plastic deformation. CFRP-only and CFRP-NSM retrofits also provided substantial improvements, offering lightweight, corrosion-resistant alternatives with effective confinement and energy dissipation. Conversely, the BSB system, while increasing overall joint capacity, revealed the potential for excessive localized plastic strains, highlighting the importance of comprehensive design and detailing to prevent premature failure. This outcome is likely linked to the inherent geometry of the bolted box, which generates hard-point stress concentrations, and to localized pinching/prying effects at the bolted interfaces. Designers considering this system should therefore exercise caution, recognizing that strength gains may be offset by concentrated damage demands unless additional measures are introduced to soften or redistribute stresses. This critical finding sets the BSB system apart from the other retrofits: while all other schemes exhibited PE maxima in the range of ~0.08–0.09, the BSB reached 0.587, nearly an order of magnitude higher. Such an anomalous response confirms that the hard-point effect of the box geometry, combined with local pinching and prying at the bolted interfaces, leads to severe strain localization. For practical design, this means that the BSB should not be applied indiscriminately and must be accompanied by refined detailing strategies (e.g., rounded edges, distributed anchorage, or composite overlays) if reliable ductility and seismic resilience are to be achieved. The detailed analysis of the maximum plastic strain index (PE) further underscored the need for integrated confinement strategies, as hybrid and composite retrofits consistently limited the progression of inelastic damage more effectively than steel-only systems. The findings of this study provide practical and quantitative guidance for engineers and decision-makers in selecting appropriate retrofit solutions for vulnerable RC frames. It should be emphasized that these conclusions are drawn from monotonic simulations, which provide valuable first-order insights into relative retrofit effectiveness. The reported improvements in “seismic performance” therefore refer to enhanced strength, ductility, and damage indices under monotonic conditions rather than full cyclic or dynamic equivalence. Future research should extend these evaluations to quasi-static cyclic and dynamic time-history analyses, optimize retrofit detailing, and integrate life-cycle cost assessments to fully support the practical implementation of advanced seismic retrofitting techniques. In particular, targeted quasi-static cyclic experiments on promising hybrid retrofit schemes (such as CFRP–NSM and CFRP–BSB) are recommended, including detailed instrumentation for joint shear, bond–slip, and PE mapping. Such tests should also incorporate specimens with intentionally imperfect bonds or anchorage details to better reflect realistic field conditions. The conclusions of this study must also be interpreted in light of several modeling idealizations, including perfect bonding assumptions between CFRP and concrete, the absence of bond–slip effects for reinforcement, and validation restricted to monotonic backbone curves. While the comparative trends are robust, the absolute claims regarding seismic resilience remain provisional. Further cyclic and dynamic analyses, combined with experimental validation, are required to confirm the extent to which the observed numerical improvements translate into actual seismic performance.

References

[1] Askar M, Abduka K, Askar L. Seismic Vulnerability Assessment of Reinforced Concrete Structures in Kurdistan Region-iraq. The Journal of the University of Duhok 2020. https://doi.org/10.26682/csjuod.2020.23.2.10.

[2] Shokrzadeh MR, Sharifi M, Nateghi Alahe F. Seismic Retrofitting of Concrete Beam-Column Connections: Numerical study FRP Strip and NSM Technique. Journal of Seismology and Earthquake Engineering 2024. https://doi.org/10.48303/JSEE.2024.2031006.1099.

[3] Shokrzadeh MR, Aziminejad A, Moghaddam AS. Evaluation of various FRP strengthening configurations for RC beam-column joints. Bridge Structures 2024. https://doi.org/10.3233/BRS-240223.

[4] Nateghi-Alahi F, Shokrzadeh MR. Behavior considerations for mechanical rebar couplers. Behavior considerations for mechanical rebar couplers, University of Tokyo: 2019, p. 30–41.

[5] Shokrzadeh MR, Nateghi-Alahi F. Experimental study of seismic behavior and modification of the failure region of mechanical bar splices. Sharif Journal of Civil Engineering 2025. https://doi.org/10.24200/J30.2024.63880.3292.

[6] Kalogeropoulos G, Tsonos AD, Iakovidis P. Hysteresis Behavior of RC Beam–Column Joints of Existing Substandard RC Structures Subjected to Seismic Loading–Experimental and Analytical Investigation. Buildings 2024, Vol 14, Page 1609 2024;14:1609. https://doi.org/10.3390/BUILDINGS14061609.

[7] Shapoori M, Sayyahi O, Jalaeefar A. Seismic performance of the exterior beam-column joint without transverse rebar using fiber-reinforced concrete and retrofit methods. Structures 2025;79:109451. https://doi.org/10.1016/J.ISTRUC.2025.109451.

[8] Khodaei M, Saghafi MH, Golafshar A. Seismic retrofit of exterior beam-column joints using steel angles connected by PT bars. Engineering Structures 2021. https://doi.org/10.1016/j.engstruct.2021.112111.

[9] Tsonos AD, Kalogeropoulos G, Iakovidis P, Bezas MZ, Koumtzis M. Seismic performance of rc beam–column joints designed according to older and modern codes: An attempt to reduce conventional reinforcement using steel fiber reinforced concrete. Fibers 2021. https://doi.org/10.3390/fib9070045.

[10] Ong CB, Chin CL, Ma CK, Tan JY, Awang AZ, Omar W. Seismic retrofit of reinforced concrete beam-column joints using various confinement techniques: A review. vol. 42. Elsevier; 2022. https://doi.org/10.1016/j.istruc.2022.05.114.

[11] Ghaderi Barmi C, Saghafi MH, Golafshar A. Seismic retrofit of severely damaged beam-column RC joints using HPFRCC. Structures 2023. https://doi.org/10.1016/j.istruc.2022.12.003.

[12] Maseer MS, Abdulridha AJ. Enhancing performance of beam-column joints in reinforced concrete structures using carbon fiber-reinforced polymers (CFRP): A novel review. Hybrid Advances 2025;10:100444. https://doi.org/10.1016/J.HYBADV.2025.100444.

[13] Shafaei J, Hosseini A, Marefat MS. Seismic retrofit of external RC beam-column joints by joint enlargement using prestressed steel angles. Engineering Structures 2014. https://doi.org/10.1016/j.engstruct.2014.10.006.

[14] Karayannis CG, Chalioris CE, Sirkelis GM. Local retrofit of exterior RC beam-column joints using thin RC jackets - An experimental study. Earthquake Engineering and Structural Dynamics 2008. https://doi.org/10.1002/eqe.783.

[15] Di Ludovico M, Balsamo A, Prota A, Manfredi G. Comparative assessment of seismic rehabilitation techniques on a full scale 3-story RC moment frame structure. Structural Engineering and Mechanics 2008. https://doi.org/10.12989/sem.2008.28.6.727.

[16] Hung CC, Hsiao HJ, Shao Y, Yen CH. A comparative study on the seismic performance of RC beam-column joints retrofitted by ECC, FRP, and concrete jacketing methods. Journal of Building Engineering 2023. https://doi.org/10.1016/j.jobe.2022.105691.

[17] Ahmadi MH, Nateghi-Alahi F. Experimental investigation of strengthening of masonry-infilled RC frames using prefabricated engineered cementitious composite panels. Engineering Structures 2022. https://doi.org/10.1016/j.engstruct.2021.113762.

[18] Shokrzadeh MR, Nateghi-Alahi F. Evaluation of hybrid NSM-CFRP technical bars and FRP sheets for seismic rehabilitation of a concrete bridge pier. Bridge Structures 2022;18:75–88. https://doi.org/10.3233/BRS-290180.

[19] Rodriguez M, Park R. Seismic load tests on reinforced concrete columns strengthened by jacketing. ACI Structural Journal 1994. https://doi.org/10.14359/4593.

[20] Ji J, Han T, Dong Z, Zhu H, Wu G, Wei Y, et al. Performance of concrete columns actively strengthened with hoop confinement: A state-of-the-art review. Structures 2023. https://doi.org/10.1016/j.istruc.2023.05.038.

[21] Bett JB, Klingner RE, Jirsa JO. LATERAL LOAD RESPONSE OF STRENGTHENED AND REPAIRED

REINFORCED CONCRETE COLUMNS. ACI Structural Journal 1988. https://doi.org/10.14359/9226.

[22] Chinthapalli HK, Chellapandian M, Agarwal A, Suriya Prakash S. Effectiveness of hybrid fibre-reinforced polymer retrofitting on behaviour of fire damaged RC columns under axial compression. Engineering Structures 2020. https://doi.org/10.1016/j.engstruct.2020.110458.

[23] Lu XZ, Teng JG, Ye LP, Jiang JJ. Bond-slip models for FRP sheets/plates bonded to concrete. Engineering Structures 2005. https://doi.org/10.1016/j.engstruct.2005.01.014.

[24] Chellapandian M, Jain S, Prakash SS, Sharma A. Effect of cyclic damage on the performance of RC square columns strengthened using hybrid FRP composites under axial compression. Fibers 2019. https://doi.org/10.3390/FIB7100090.

[25] Chellapandian M, Prakash SS. Rapid repair of severely damaged reinforced concrete columns under combined axial compression and flexure: An experimental study. Construction and Building Materials 2018. https://doi.org/10.1016/j.conbuildmat.2018.04.037.

[26] Jain S, Chellapandian M, Suriya Prakash S. Emergency repair of severely damaged reinforced concrete column elements under axial compression: An experimental study. Construction and Building Materials 2017. https://doi.org/10.1016/j.conbuildmat.2017.08.127.

[27] Zhang D, Li N, Li ZX, Xie L. Rapid repair of RC bridge columns with prestressed stainless-steel hoops and stainless-steel jackets. Journal of Constructional Steel Research 2021. https://doi.org/10.1016/j.jcsr.2020.106441.

[28] Janke L, Czaderski C, Ruth J, Motavalli M. Experiments on the residual load-bearing capacity of prestressed confined concrete columns. Engineering Structures 2009;31:2247–56. https://doi.org/10.1016/j.engstruct.2009.04.006.

[29] Rousakis TC, Tourtouras IS. RC columns of square section - Passive and active confinement with composite ropes. Composites Part B: Engineering 2014. https://doi.org/10.1016/j.compositesb.2013.11.011.

[30] Ilki A, Tore E, Demir C, Comert M. Seismic performance of a full-scale frp retrofitted sub-standard RC building. Geotechnical, Geological and Earthquake Engineering, 2018. https://doi.org/10.1007/978-3-319-75741-4_22.

[31] Du YX, Shao X, Chu SH, Zhou F, Su RKL. Strengthening of preloaded RC beams using prestressed carbon textile reinforced mortar plates. Structures 2021. https://doi.org/10.1016/j.istruc.2021.01.024.

[32] Rezaie F, Farnam SM, Pour Bahar S. Numerical Analysis of Reinforced Concrete Beam-Column Joints without Transverse Reinforcement. Numerical Methods in Civil Engineering 2022. https://doi.org/10.52547/nmce.2022.238.

[33] Shrestha R, Smith ST, Samali B. Strengthening RC beam-column connections with FRP strips. Proceedings of the Institution of Civil Engineers: Structures and Buildings 2009. https://doi.org/10.1680/stbu.2009.162.5.323.

[34] Kent DC, Park R. Flexural Members with Confined Concrete. Journal of the Structural Division 1971. https://doi.org/10.1061/jsdeag.0002957.

[35] ABAQUS, Simulia, ABAQUS. Abaqus User's Manual version 2019. Dassault Systèmes Simulia Corp: Providence, RI, USA 2019.

[36] ACI 318-19 Building Code Requirements for Structural Concrete and Commentary. 318-19 Building Code Requirements for Structural Concrete and Commentary 2019. https://doi.org/10.14359/51716937.

[37] Mohamad Reza Shokrzadeh, A.M.Oveyci, R.Pourmirza, M.Shaifi. Seismic Retrofitting of Concrete Beam-Column Connections Using FRP Strip and CFRP Bar with NSM Technique. Conference: 9th International Conference on Seismology and Earthquake Engineering (SEE9), 2024.

[38] shokrzadeh mohamad reza, aziminejhad armin. Investigating of the Performance of Different Diagonal Brace Patterns in Rehabilitation Lightweight Steel Frame (LSF). Analysis of Structure and Earthquake Vol 1 1 2018;1:1.

[39] Y. sumer. Defining parameters for concrete damage plasticity model. Challenge Journal of Structural Mechanics 2015. https://doi.org/10.20528/cjsmec.2015.07.023.

[40] Kent DC, Park R. FLEXURAL MEMBERS WITH CONFINED CONCRETE. Journal of the Structural Division 1971.

[41] Vilanova I, Torres L, Baena M, Llorens M. Numerical simulation of bond-slip interface and tension stiffening in GFRP RC tensile elements. Composite Structures 2016;153:504–13. https://doi.org/10.1016/j.compstruct.2016.06.048.

[42] Shokrzadeh MR, Nateghi-Alahi F. Experimental study of seismic behavior and modification of the failure region of mechanical bar splices in reinforced concrete vertical elements. Sharif University of Technology, 2024. https://doi.org/10.24200/J30.2024.63880.3292.

[43] Mohamad Reza Shokrzadeh AA. Numerical modeling of reinforced concrete joints reinforced with FRP in software ABAQUS. 2017/1/26, 2017, p. 10–22.

[44] Barros JAO, Fortes AS. Flexural strengthening of concrete beams with CFRP laminates bonded into slits. Cement and Concrete Composites 2005. https://doi.org/10.1016/j.cemconcomp.2004.07.004.

[45] Sena Cruz JM, Barros JAO, Gettu R, Azevedo ÁFM. Bond Behavior of Near-Surface Mounted CFRP Laminate Strips under Monotonic and Cyclic Loading. Journal of Composites for Construction 2006. https://doi.org/10.1061/(asce)1090-0268(2006)10:4(295).

[46] Coronado CA, Lopez MM. Sensitivity analysis of reinforced concrete beams strengthened with FRP laminates. Cement and Concrete Composites 2006. https://doi.org/10.1016/j.cemconcomp.2005.07.005.

[47] Rong B, Sun J, Xu M, Zhang R, Sun Y, Zhang W, et al. Experimental and numerical investigation on seismic performance of S-RC-SRC composite joint. Journal of Building Engineering 2021. https://doi.org/10.1016/j.jobe.2021.103079.

[48] Torra-Bilal I, Mahamid M, Bilal K. Performance of Precast Connections on a Moment Resisting Frame under

Cyclic Loading. Structures Congress 2019: Blast, Impact Loading, and Research and Education - Selected Papers from the Structures Congress 2019, 2019. https://doi.org/10.1061/9780784482247.031.

[49] Shokrzadeh MR, Nateghi-Alahi F, Mansoori MR, Javadi P. The improvement of the threaded-based mechanical splice by modifying the threaded system: Study of techniques cold rolling and rotating friction welding. Journal of Building Engineering 2023;80:107964. https://doi.org/10.1016/J.JOBE.2023.107964.

[50] Shokrzadeh MR, Nateghi Allahe F, Mansoori , Mohammad Reza, Javadi P, Mansoori, MR, Javadi P. Failure area evaluation of the coupler with threaded bar: Experimental and Numerical study. International Journal of Advanced Structural Engineering 2022;12:531–43. https://doi.org/10.1007/IJASE.2022.692294.